SPECTROSCOPIC MEASUREMENTS OF NATURAL AND ARTIFICIAL LIGHT SOURCES

THESIS

Presented to the Graduate Council of
Texas State University-San Marcos
in Partial Fulfillment
of the requirements

for the Degree

Master of SCIENCE

by

Sagar Ghimire, M.S.

San Marcos, Texas
August, 2010

SPECTROSCOPIC MEASUREMENTS OF NATURAL AND ARTIFICIAL LIGHT SOURCES

Committee Members Approved:

_____
Karl D. Stephan, Chair

_____
Eulogio Velasco

_____
Wilhelmus J. Geerts

Approved:

_____
J. Michael Willoughby
Dean of the Graduate College

ACKNOWLEDGEMENTS

I would like to thank my major advisor Dr. Karl D. Stephan for his guidance, support and help throughout my master's study. His expertise and experience made my interest grew in the fields of plasma science and spectroscopy. I am also very thankful for the innovative research environment he created in the laboratory. I would also like to thank Dr. Velasco and Dr. Geerts for being on my committee and providing me with constructive remarks and suggestions.

Our field experiment in the Marfa-Alpine areas would not have been completed without help from Ms. Pamela Stephan and Mr. Benjamin Simons. I appreciate their much needed logistical help. I also thank Mr. James Bunnell for helpful discussions.

I am very grateful to both the Department of Engineering Technology and the Ingram School of Engineering for providing me with a graduate assistantship. I am grateful to the Graduate College and the Associated Student Government for providing me with scholarships. I am also thankful to my graduate advisor Dr. Batey for his guidance.

I would like to thank my family for their support and love. Finally I am very grateful to my wife Anita for her support.

This manuscript was submitted on March 25, 2010.

TABLE OF CONTENTS

Page

LIST OF FIGURES

Figure **Page**

ABSTRACT

SPECTROSCOPIC MEASUREMENTS OF NATURAL AND ARTIFICIAL LIGHT SOURCES

by

Sagar Ghimire, M.S.

Texas State University-San Marcos

August 2010

SUPERVISING PROFESSOR: KARL D. STEPHAN

A twenty-night field investigation at the site where reportedly Marfa lights have most been observed was conducted. We made considerable progress in developing a technique to identify false positives and to estimate their distance based on the absorption of molecular oxygen at 762 nm band using the spectroscopic data alone (Stephan, Ghimire, Stapleton, & Bunnell, 2009). Spectroscopic studies of a type of glow discharge supported by natural porous rock which covers relatively wide area of the rock, up to 2 cm in diameter, are presented. The rotational, translational and vibrational temperatures of the discharge are measured by comparing modeled optical emission spectra with spectroscopic measurements from the discharge. Finally, an absolute calibration technique for our spectroscopic system is presented.

I. INTRODUCTION

Most naturally occurring light sources have been identified, extensively studied and understood scientifically. Franklin studied the lightning phenomenon and proved that it is a natural electrical discharge, and was able to reproduced lightning on a small scale in the laboratory. Physicists were able to describe light's behavior by using Maxwell's equations in a quantitative way. In the twentieth century, with the advent of the quantum mechanics, understanding of how light is produced in nature was almost complete.

There are few natural occurring light-producing phenomena that lack a complete comprehensive explanation which accounts for their unique characteristics and would also permit their reproduction in the laboratory. One of the most well known of such phenomena is ball lightning. People have reported seeing ball lightning for hundreds of years (Abrahamson, Bychkov, & Bychkov, 2002). But scientists still can't explain what causes it, or even exactly what it is. Although there have been numerous articles, publications, and seminars on the phenomenon of ball lightning and fireballs, only a very few have ever reported on the actual production of ball lightning. Yet even fewer of these handfuls have ever actually produced fireballs under conditions that could be considered similar to nature. There are thousands of witnesses who have seen ball lightning and some people who have taken photographs. Another case of recurring unexplained light phenomena are the so-called Marfa lights. Marfa lights are points or spheroids of light that appear in a restricted geographical area between Marfa and Alpine, Texas. These lights may or may not be related to ball lightning and are not as well

accepted as an unexplained phenomenon compared to ball lightning. However, they are more predictable in their occurrence. The only publication on this subject addressed primarily to a scientific audience, before our twenty-night field investigation (Stephan, et al., 2009), was a report of a two-night investigation carried out by the Society of Physics Students at the University of Texas at Dallas (Stolyarov, Klenzig, Roddy, & Heelis, 2005).

Both Marfa lights and ball lightning studies so far lack good-quality experimental and observational evidence mainly because of the following two reasons. First, scientific data on natural ball lightning and Marfa lights are scarce owing to unpredictability. We are unaware of any effort to obtain scientific data on ball lightning because the resources required are very expensive. Also, most of the data gathered from eyewitness accounts are not scientific as most of the witnesses are not scientifically trained observers. In the case of Marfa lights there has been enough observational work done which suggests a "true" Marfa light event occurs at most between two to three times in a year. This implies that a long-term effort is required to collect the observational data. Secondly, the available data are not of scientific quality. The photographs of ball lightning could not even yield basic data about the spectral shape. This same problem occurs in the case of Marfa lights.

In this thesis we have two different but related attempts to obtain quantitative spectroscopic data that will enable us to theorize about the nature of ball lightning and Marfa lights in a more disciplined and scientific way. Spectroscopy is the science of using spectral analysis to figure out what something is made of. Spectra are very powerful tools in studying astronomical objects and plasmas because they represent the

signature pattern of the source of light. The light we see is composed of a mixture of wavelengths. We can separate the light into its component wavelengths (spectrum) by passing it through a dispersing element such as a diffraction grating or a prism. There are two basic types of spectra: continuous spectra and line spectra. Continuous spectra originate from heated solids such as the heated tungsten filament in incandescent light bulbs. Line spectra originate from individual atoms such as in low pressure gas discharge lamps. Line spectra are specific for a certain elements and provide us a means to determine the atomic composition of the source.

The thesis is divided into two parts. In the first part, we describe a 20 night field experiment conducted at the Marfa Light View Park, during which we obtained spectra of several objects, such as automotive headlights, some of which could have been mistaken for lights of unknown origin by casual observers. The Marfa lights are reported to be seen in or near Mitchell Flat, an area between Alpine and Marfa in Texas (Bunnell, 2009). Many people have reported seeing them. They are yellowish-white lights that glow, fade, disappear, and return in different places (Hall, 2006) . Although we did not see any "genuine" Marfa lights, spectroscopic analysis of the visible oxygen absorption band near 13121 cm^{-1} (762 nm) was used to derive an algorithm to estimate distances to automotive headlights with a continuum spectrum (Stephan, et al., 2009). This technique can be used to estimate distances to the false positives from the spectroscopic data alone. This distance measuring algorithm could be used to estimate distance to other light sources of unknown origin with a continuum spectrum as well.

The second part of the thesis describes a study of a type of glow discharge supported by natural porous rock. One explanation for luminous objects that are excited

by electric fields is called St. Elmo's fire – a kind of corona discharge. Some eyewitness accounts of ball lightning may be corona discharge; however, there is very little scientific literature about the mechanism by which corona may appear visible on the surface of the ground. We attempted to investigate this phenomenon experimentally in laboratory settings. We discovered that many types of moist porous rocks support a type of DC glow discharge that has been identified in laboratory settings with artificial materials. However, it is not clear what are the conditions required for this type of normal glow discharge to occur in nature. There has been considerable industrial interest in generating large volume (diffuse) discharges at atmospheric pressure. Although these plasmas can be produced between metal electrodes (Staack, Farouk, Gutsol, & Fridman, 2005), they are typically small with diameter less than 200 μm. The most important observation that we made regarding the glow discharges in porous rock is the fact that it covers a surface area up to 2 cm in diameter. This is unprecedented in the literature and therefore we are in the process of completing a paper on this matter. Also, from the spectroscopic analysis of the glow discharges we have found that it is essentially a low-temperature plasma, which may have useful applications in industries. A program called SPECAIR, which does sophisticated modeling of atmospheric spectra, has been used to compare our experimental results with the simulated model spectrum.

SPECAIR is a program for modeling the absolute intensity spectral radiation emitted by gases and plasmas of various compositions. It can model 37 molecular transitions as well as atomic lines of N,O, and C (Laux, Spence, Kruger, & Zare, 2003). It lets us choose translational, electronic, vibrational and rotational temperatures individually. The code then uses Boltzmann distributions of the electronic, vibrational,

and rotational temperatures to determine the population of the internal energy levels. SPECAIR also allow us to take into account the effect of absorption by room air between the emitting gas or plasma and the detector.

An important issue discussed in this thesis is the calibration of our spectroscopic system. Much effort is needed for the absolute calibration of the intensity axis. A relative calibration takes into account only the spectral sensitivity of the spectroscopic system along the wavelength axis. An absolute calibrated system provides calibrated spectra, which gives direct access to plasma parameters (Fantz, 2006). Thus, our effort will be rewarded by an increase in information. One of the most critical steps in the calibration procedure is the imaging of the light source to the spectroscopic system. We must be very careful to conserve the solid angle. Although our efforts to calibrate our spectrometer are incomplete, we present a theoretical framework for carrying out such calibration in the final portion of this thesis, along with some experimental data.

II. METHODOLOGY

Experiment I: Distance Estimation Using Oxygen Absorption Band

A simplified system diagram is shown in Figure 1. Besides optical spectra, we recorded video images of the object of interest with all data time-stamped with the precise time data available from a GPS receiver (Stephan, et al., 2009).

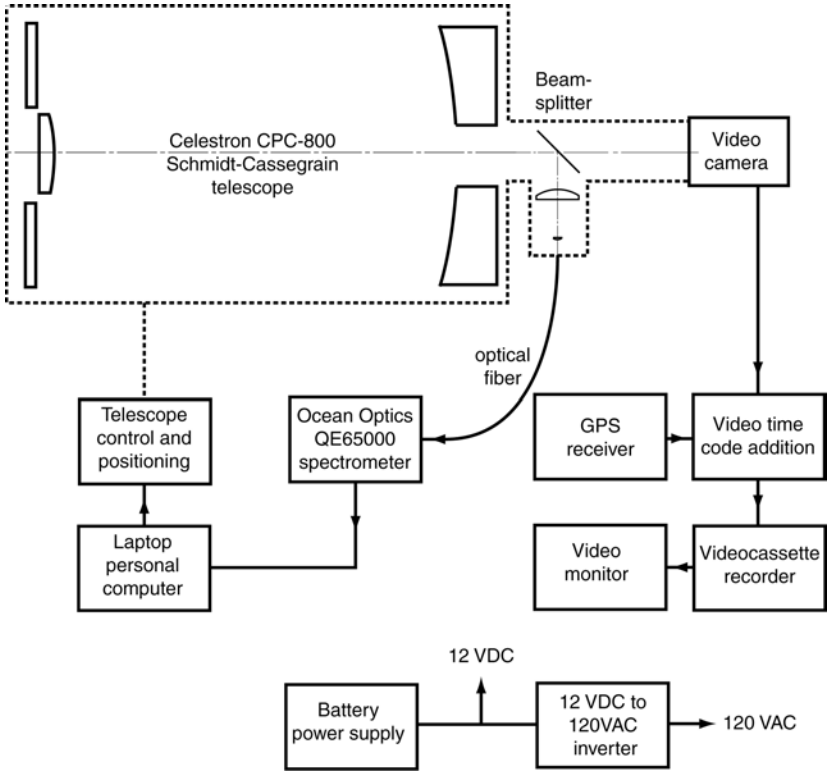

Figure 1. Simplified system diagram of telescope-camera-spectrometer setup

The telescope is a Celestron CPC-800 Schmidt-Cassegrain design with a 203-mm aperture. It was equipped with a 1-X finding sight and 8-X finding scope used for initial sighting of objects of interest (see Figure 1). A splitter/imager system was attached to the

visual back of the telescope. The splitter/imager used a 75%-reflectivity beamsplitter mirror that directed most of the incoming light to two plano-convex lenses, which focused the beam onto a 1-mm-diameter fiber-optic cable leading to an Ocean Optics QE65000 CCD-array spectrometer. The spectrometer can produce a resolution of about 3 nm when resolving a single atomic line. The size of the image produced by the splitter/imager on the fiber end was designed so that 50% or more of the peak on-axis optical power from a point source would enter the fiber as long as the telescope was pointed to within ±5 arcmin of the source. Since the video camera used a 1/3-inch chip giving a field of view that was approximately 5 by 7.5 arcmin, the fiber image size ensured that any luminous source visible through the camera could also produce a spectrum, assuming its intensity was sufficient.

The spectrometer was monitored with a laptop computer. The telescope control was manual, although an automatic tracking feature could easily be incorporated without much additional hardware. Custom software was used to monitor azimuth and altitude data from the telescope's motorized elevation-azimuth mount every 0.7 seconds. The position data were time stamped with GPS-synchronized time codes.

The spectrometer was set to capture spectrum covering the 200-900 nm range. Exposure time of 10 seconds was found to be adequate for capturing spectrum of dim objects without saturating the CCD on bright objects.

Power sources were one of the important considerations for our field experiment because commercial power was not available. We used a 12-V 110-AH deep-discharge lead-acid battery. This allowed continuous operation of our setup for at least 5 hours. Initially we used two 17-AH 12-V power packs using gel-type lead acid batteries, but these proved to be inadequate.

Molecular oxygen has a spectroscopic absorption band near the 762 nm (13121 cm^{-1}) region as shown in Figure 2. This band was first noted by Fraunhofer in the solar spectrum and is often referred to as the Fraunhofer *A* band.

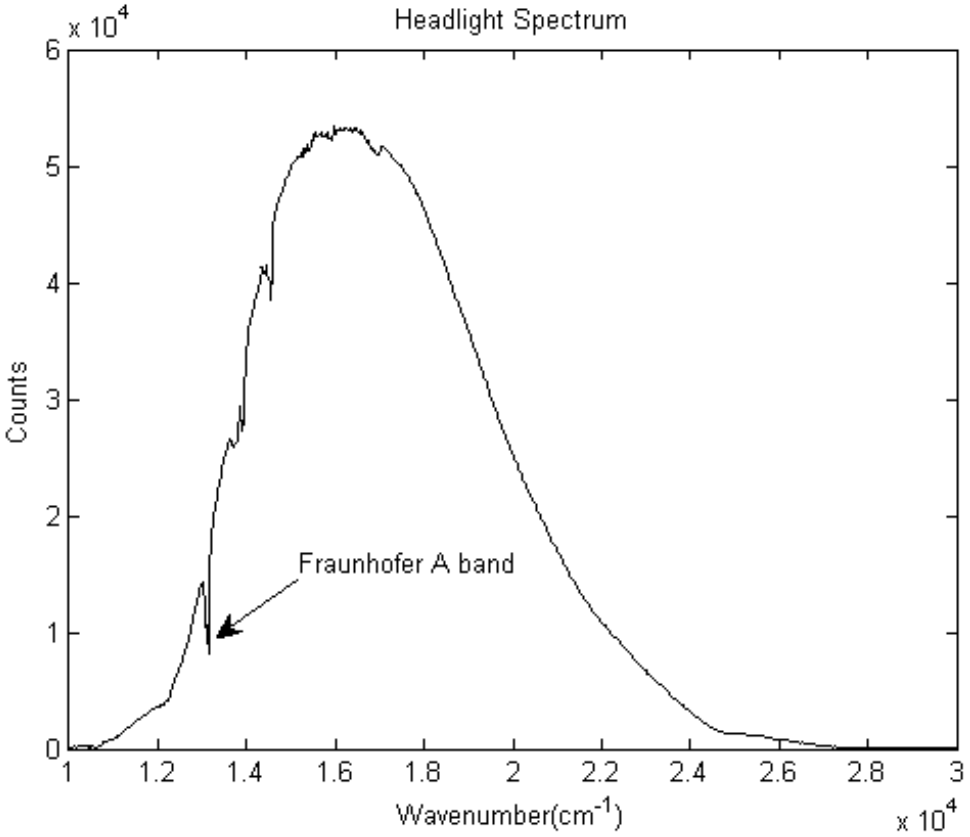

Figure 2. Headlight spectrum obtained on 24 May 2008 and corrected only for zero offset.

Because the depth of the absorption "notch" caused by this band is a monotonically increasing function of the optical depth of the atmosphere between the source and the observer, it has been used for various remote-sensing purposes such as determining cloud heights from satellites (Pierluissi & Tsai, 1986; Wark & Mercer, 1965). Sufficient absorption occurs in this band over path lengths as short as 1 km to permit estimation of the source-to-observer distance of continuum sources. Our distance-estimation algorithm is a two-step process.

In the first step, the experimental data points that lie outside absorption bands were used to obtain a cubic polynomial $P(\upsilon_i)$ fit to a small portion of the underlying continuum spectrum as shown in Figure 3 (Stephan, et al., 2009). The cubic polynomial model is our model for the source spectrum as it would appear to our spectrometer without the absorption bands. We used this polynomial to transform our raw data into an experimental transmission function τ_{EXP} whose value outside the absorption bands is approximately unity. If the raw spectrometer data in counts per wavenumber pixel after subtracting dark-spectrum background are designated as $D(\upsilon_i)$, then the experimental transmittance function is

$$\tau_{EXP}(\upsilon_i) = \frac{D(\upsilon_i)}{P(\upsilon_i)} \tag{1}$$

The experimental transmission function for each of N=32 wavenumbers covering the Fraunhofer A absorption band , specifically from 13267 cm^{-1} to 12870 cm^{-1} is computed. These 32 data-points correspond to the 32 pixels provided by the QE65000

spectrometer output in the selected band. The pixels are spaced about 0.75 nm apart in this region.

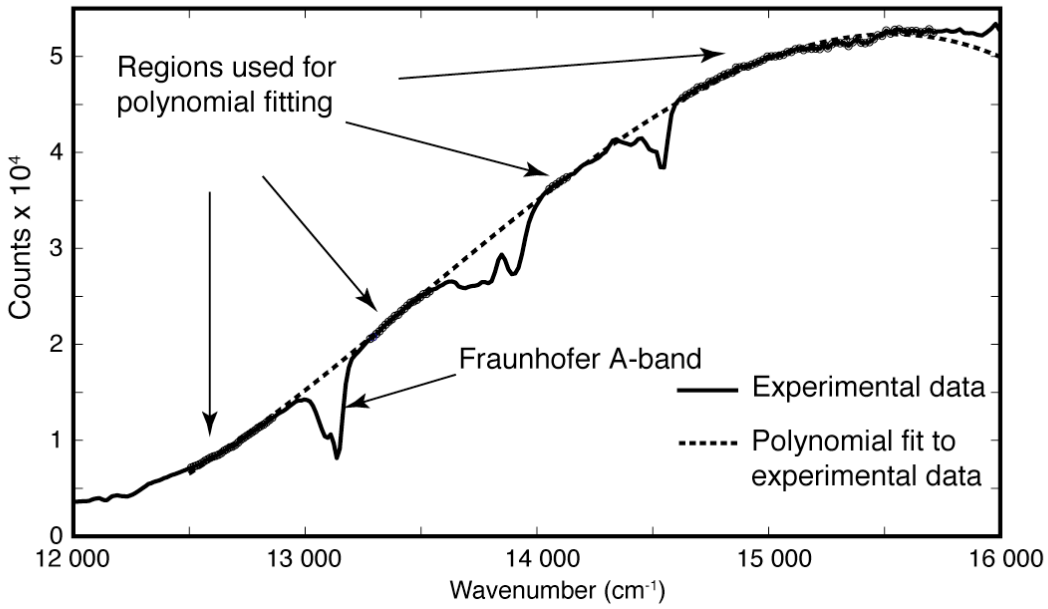

Figure 3. Polynomial fit to the experimental data

Using expressions and tables derived by (Pierluissi & Tsai, 1986) for their model of atmospheric transmittance in the *A* band, we used the variables of atmospheric pressure, temperature, and optical path length to obtain a predicted or model transmission function τ_{MOD}. Next, we adjusted the optical path length used in the model transmission function until the root-mean-square error between the experimental and model transmission functions was minimized. Figure 4 shows the modeled and the derived or experimental transmission functions.

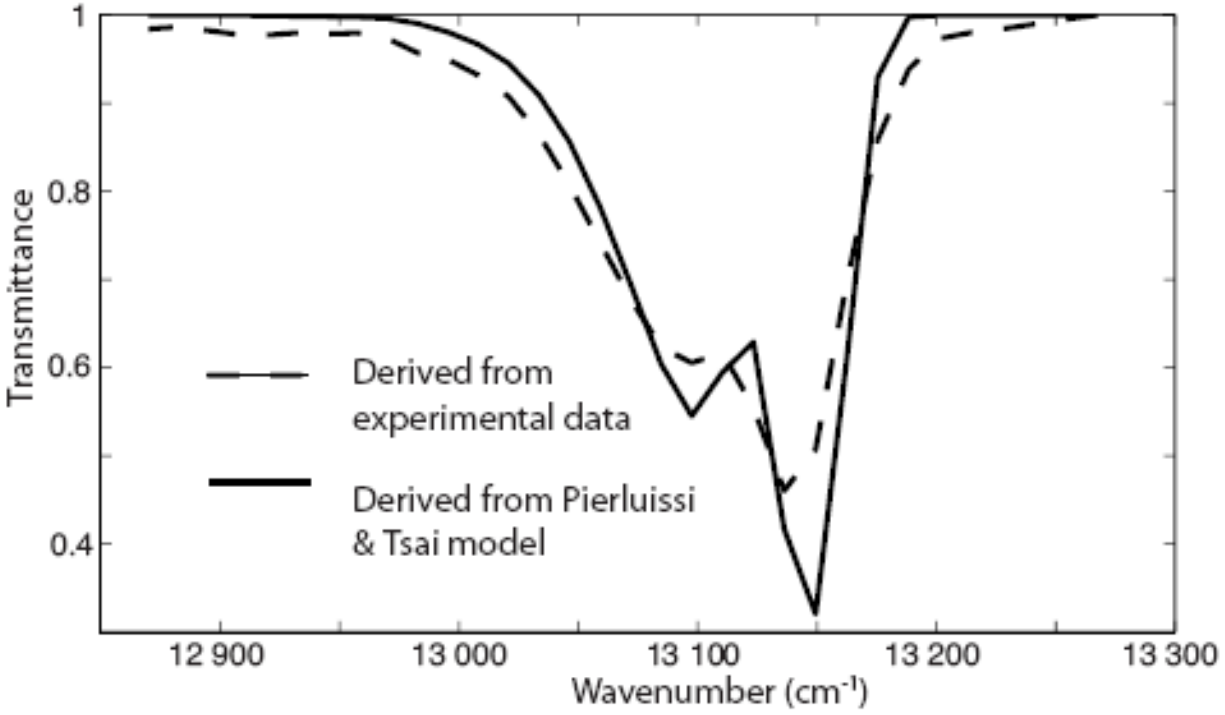

Figure 4. Comparison of the transmission function derived from experimental data and the model transmission function of Pierluissi and Tsai for d=4.57 KM

The path length that gives the minimum root-mean-square error between the two functions is the estimated distance to the source. This is shown in Figure 4 (Stephan, et al., 2009). The RMSE as a function of distance *d* can be expressed as

$$\varepsilon(d) = \left[\frac{\sum_{i=1}^{N} (\tau_{EXP}(\upsilon_i, d) - \tau_{MOD}(\upsilon_i, d)}{N} \right]^{1/2} \quad (2)$$

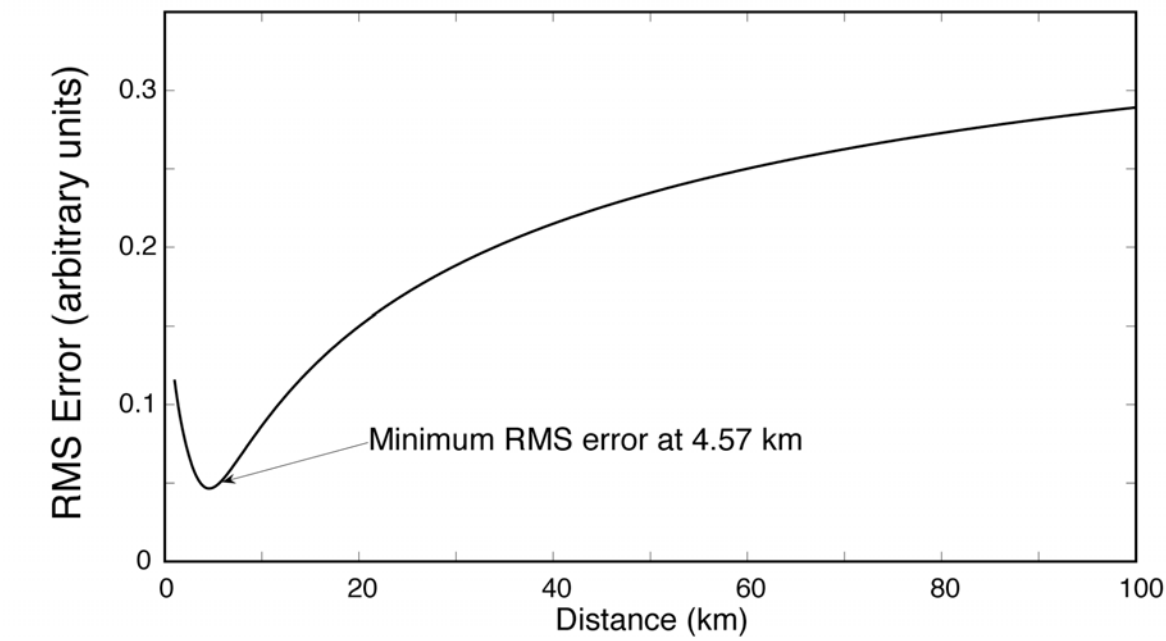

Figure 5. Root-Mean-Squared Error for an object at approximately 4.57 km from the observer

This algorithm produces a reasonably accurate estimate of the optical path length, which converts directly to distance if the atmospheric conditions are known. When a source is known to be located on a road, its location can often be established independently by means of GIS and azimuth data. In these cases we can compare the distance calculated by the atmospheric oxygen-band absorption and GIS-azimuth approaches. The RMSE in (2) as a function of distance *d* for an observation of headlights on 24 May 2008 at 21:20:35 CDT is shown in Figure 5 (Stephan, et al., 2009). The minimum value of RMSE is at 4.57 km.

The result of this experiment is presented in the results section later.

Experiment II: Atmospheric-Pressure DC Glow Discharge

The generation of uniform glow discharges in open air is a remarkable achievement in plasma field research. Uniform and stable glow discharges without additional flowing gases and a vacuum chamber eliminate the need for low-pressure technology and vacuum-compatible materials, and can be applied to plasma applications such as surface modification, thin film deposition and etching used in the semiconductor industry, cleaning, removing pollutant gases, and sterilization (Garamoon & El-zeer, 2009; Staack, et al., 2005).

One of the most studied non-equilibrium plasma discharge is the low pressure normal glow discharge. We investigated the spectra of atmospheric pressure DC normal glow discharge in air. The setup as shown in Figure 6 was used. The power supply was connected in series to the ballast resistor and the discharge gap. When the power supply voltage is in excess of the breakdown voltage for the gap the discharge initiates. The ballast resistor of 400 kΩ serves to stop the current from increasing too much. At breakdown the plasma discharge has a negative differential resistance because as the discharge transition to a self sustained mode and the current rapidly increases, the voltage required to maintain the plasma actually decreases since the gas in the discharge gap has become more conductive.

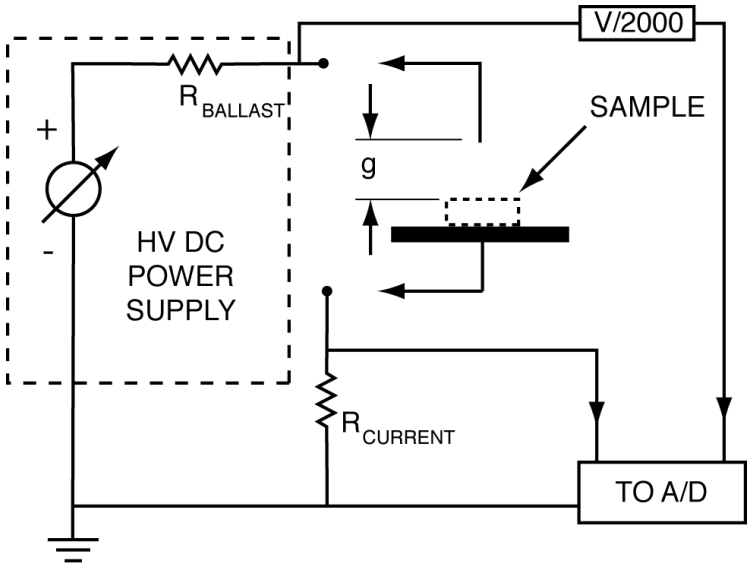

Figure 6. Experimental setup to produce DC atmospheric pressure normal glow discharge

The power supply used was an unregulated Cockroft-Walton-type voltage-multiplier-rectifier capable of producing in excess of 50 kV at a maximum current of about 5 mA. Since it lacks electronic regulation, its output characteristic is not that of a voltage source, but closer to that of a nonlinear current source. The positive high-voltage output of the supply was monitored by a high-power 25-MΩ voltage-divider resistor, which formed part of the divide-by-2000 voltage sensing circuit shown. The current drawn by the discharge was monitored by observing the voltage across the resistor $R_{CURRENT,}$ which was 1 kΩ for the monitoring of continuous currents and 50 Ω for observations of large impulse currents greater than 10 mA. The discharge took place between 1.6-mm-diameter pure tungsten or stainless-steel rod and a sample of basalt about 3 cm thick x 5.5 cm x 10 cm, polished on the upper side. All tests on this sample were made with the electric field parallel to the 3-cm axis. The basalt sample rested on a disc-shaped copper plate with rounded edges, covered with aluminum foil. The gap

length *g* between the rod and the basalt surface was set directly by a micrometer-driven translation table 5 for distances up to 20 mm, and by direct manual micrometer measurements of the gap for distances in excess of this. Probable accuracy of the gap distance setting was about ±0.5 mm. Both the rod and the disc electrodes were insulated to a test potential of more than 50 kV to ground in order to allow either electrode to be used as the positive terminal, since the power supply's high-voltage terminal polarity was fixed as positive. Leads from the electrodes to the power supply were detachable as indicated by arrows in Figure 6, allowing for reversal of electrode polarity. Voltage and current data were digitized with either a National Instruments LabView™ 12-bit A/D converter for low-speed data acquisition (up to 10 points/sec), or a Tektronix TDS2014B 100-MHz digital oscilloscope for high-speed acquisition. A non-metallic 200-μm diameter fiber-optic cable was used to convey light originating within its acceptance angle cone (full width = 50.8 degrees) to an Ocean Optics QE65000 CCD-array spectrometer. A photograph of the sample resting between the rod electrode and the plate electrode is shown in Figure 7.

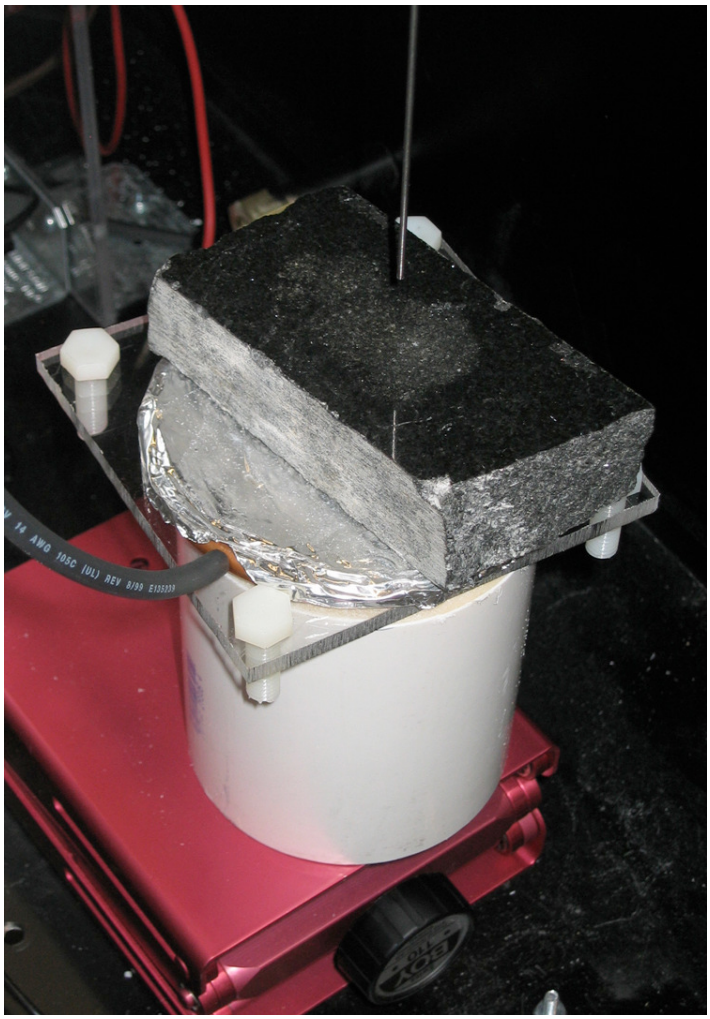

Figure 7. Basalt sample resting on disc electrode, supported beneath rod

Structure of the Normal Glow Discharge

The structure of the DC glow discharge is well studied. Figure 8 shows the structure of the DC glow discharge. In atmospheric pressure normal glow discharges mostly the negative glow, Faraday dark space and positive column are clearly visible. We will describe these basic structures starting from the cathode and proceeding towards the anode.

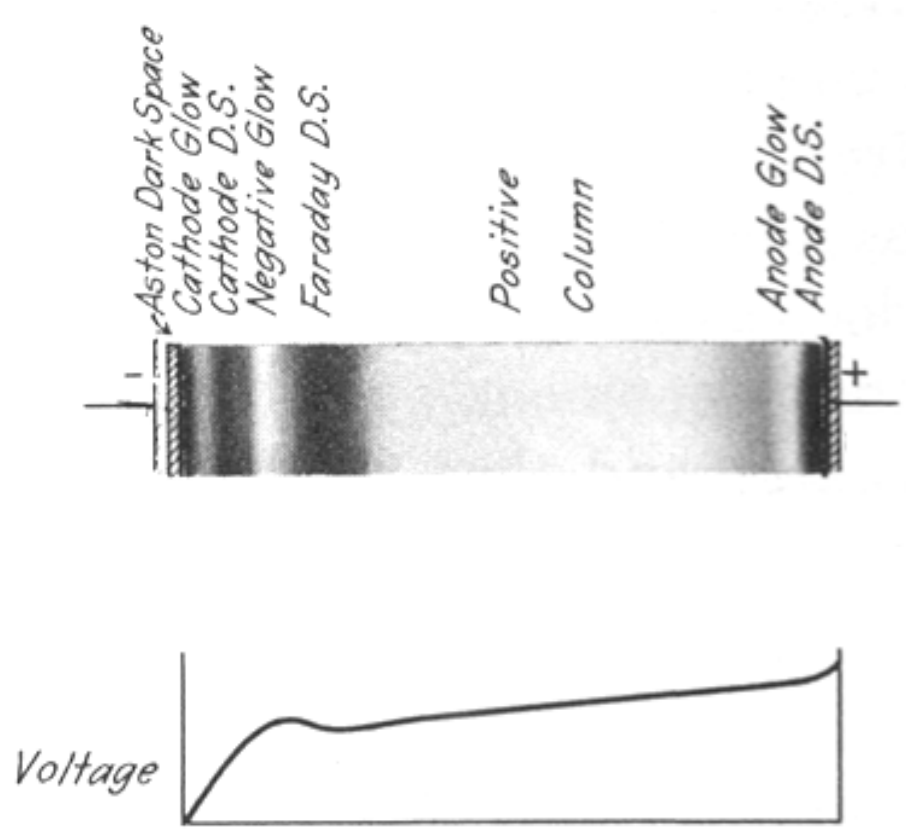

Figure 8. **Structure of a DC glow discharge (it is "adapted from J. D. Cobine, *Gaseous Conductors* (NY: Dover, 1958), fig. 8.4")**

Cathode. It is an electrical conductor with a secondary emission coefficient which is very important for the operation of the glow discharge. Secondary electron emissions occur at the cathode due to ion flux on its surface.

Cathode glow. The next important structure adjacent to the cathode is the cathode glow. In this region, electrons are energetic enough to excite the neutral atoms they collide with. The cathode glow has a relatively high ion density. Its axial length depends upon the surrounding gases and the pressure.

Faraday dark space. The energy of the electrons are very low in this region. The electron number density decreases by recombination and diffusion to the walls, the net space charge is very low, and the axial electric field is small.

Positive glow. The electric field is just large enough to maintain a constant degree of ionization along its length. In air the color of the positive column plasma is pinkish blue. As the length of the discharge tube is increased at constant pressure, the length of the cathode structures remains constant and the length of the positive column increases. The positive column is a long, uniform glow. Incredibly long positive columns can be created, for example in the case of neon tubes.

Striations. Moving or standing striations are traveling perturbations in the electron number density which occurs in partially ionized gases. The moving striations are propagating bands which appear in positive columns.

Temperature Measurement Using Emission Spectroscopy

The main objective was to use the optical emission spectroscopy to measure the rotational and vibrational temperature of the glow discharge using the N_2 second positive system (N_2 $C^3\Pi_u$ $^-B^3\Pi_g$). This transition is chosen because the N_2(C-B) transition can be seen independent of other transitions for different species and electronic states. A Boltzmann distribution is assumed with a rotational temperature T_{rot}. The rotational and translational temperatures T_{tran} were assumed equal. This is valid considering the short times of rotational to translational energy transfer. A program called SPECAIR is used to model spectra of the anode glow, the cathode glow and the positive column. The temperature measurements were made by computing the RMS error (RMSE) between our

measurements and the model at 28 wavelength points encompassing the transition in question. We considered a subset between 360.44 and 381.79 nm from our QE65000 spectrometer data on a single vibrational band centered at 375 nm. Since our spectrometer is not absolutely calibrated, this window of 21.35 nm will provide better accuracy since the quantum efficiency is relatively constant in this small range. The apparatus line broadening was taken into account by convolving the modeled narrow-line spectra from SPECAIR with the instrument slit function. A spectrum from a calibrated mercury light source was used to compute the slit function. The search for the best-fit conditions was computed using a MATLAB script. We find that there are measureable temperature differences between different parts of the discharge as discussed in the next section.

III. RESULTS

Experiment I

The comparisons of distance measurements using the oxygen absorption band and GIS is shown in the Table 1. They agree within 1.4 km or better (Stephan, et al., 2009).

Table 1. Comparison of Distances measured by Oxygen Absorption and GIS

Date (CDT)	Distance Z_S (km) computed from 762-nm absorption spectrum	Distance Z_G (km) computed from azimuth and GIS data	Difference Z_S - Z_A (km)
May 14	34.3	35.65	-1.35
May 22	35.7	34.42	1.28
May 24	4.57	4.73	-0.16
May 24	4.1	4.36	-0.26
May 24	4.1	4.36	-0.26
May 26	0.46	0.21	0.25

We were able to estimate the distance between the distant optical source and the spectrometer by minimizing the RMSE values for various distances. The minimum-error value of distance is the most likely distance to the source, based upon spectroscopic observation of the oxygen absorption band. This is verified independently using GIS software.

Experiment II

Photographs of the discharge were taken with a MIRO Phantom 640x480-pixel high-speed video camera. The photographs taken at speeds as high as 500 fps show that the discharge is wide and steady. Figure 9 shows a discharge as it appears with a current of 5.1 mA and a gap length of 30 mm. A small bright-blue cathode spot usually appears directly on the lower surface of the tungsten rod, but is positioned on the rod so as not to be visible in Figure 9. Beneath the cathode spot a long pinkish positive column with one or more stable striations extends downward toward the basalt surface.

The visible width of the positive column, as measured between half-intensity points on the photo, increases from 800 μm at the widest part of the upper bright region to about 1000 μm at the widest part below the second striation, where the glow fades into invisibility. This positive column is not always perfectly stationary. Its motion was restricted to less than a cm in directions transverse to the electric field, and was accompanied by minor shifts in the discharge current.

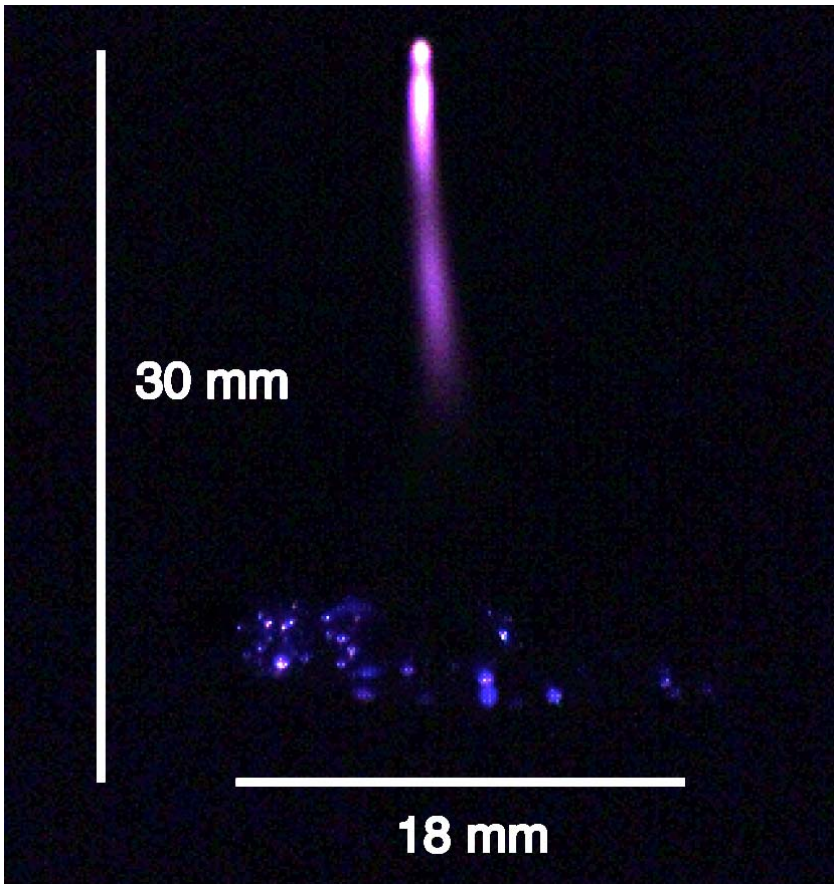

Figure 9. Photo of 30-mm-long DC atmospheric-pressure normal glow discharge in air. Current 5.1 mA, voltage 11.4 kV. Note pinkish positive column with two stable striations, and numerous anode glows on surface of basalt in circle approximately 18 mm in diameter.

A room-light view of the same electrode-rock configuration with no discharge occurring is shown in Figure 10.

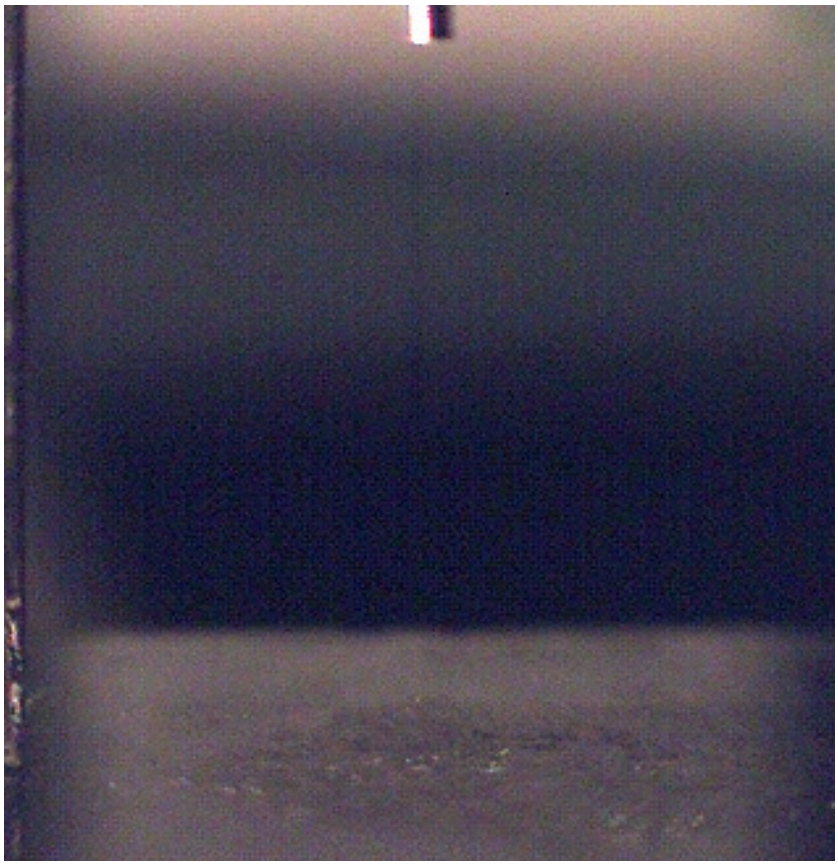

Figure 10. Room-light view of tungsten electrode and basalt surface

The most interesting aspect of the discharge occurs between the end of the visible portion of the positive column and the surface of the basalt sample. The blue anode glows of varying brightness appear over a circular field which was up to 18 mm in diameter or more, as shown in Figure 9. This is evidence that plasma current from this discharge widens out at the anode end to cover the 1-2 cm diameter of the illuminated circle. Shorter gap lengths cause the circle's diameter to decrease. There was a visible circle at least a few mm wide for gaps as short as 10 mm.

Figures 11, 12 and 13 show the measured spectra and the corresponding best-fit modeled spectra for different regions of a 13-kV, 3-mA discharge through a 25-mm air gap between a stainless steel negative electrode and the basalt positive electrode for spectra centered around 375 nm. The transitions around 375 nm are used because they are more intense, and they allow us to determine T_{rot} and T_{vib} more precisely compared to the transition at 313 nm.

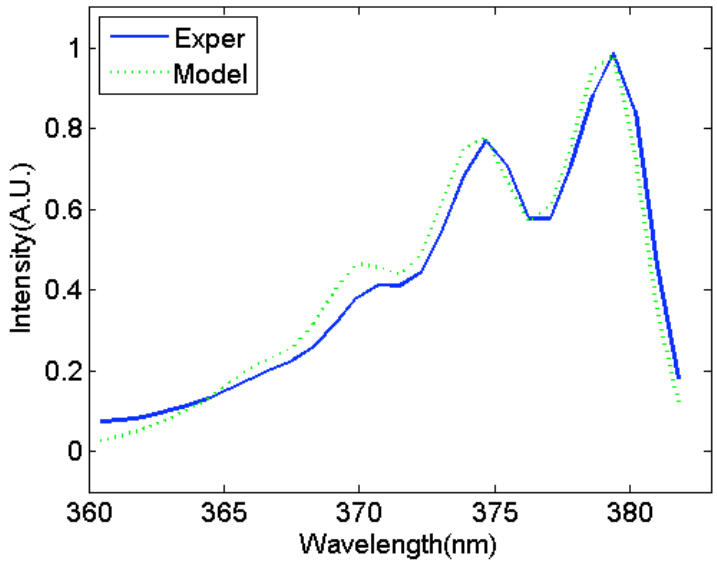

Figure 11. Modeled spectra and the corresponding best-fit for cathode glow (T_{rot} = 1500 K, T_{vib} = 3000 K)

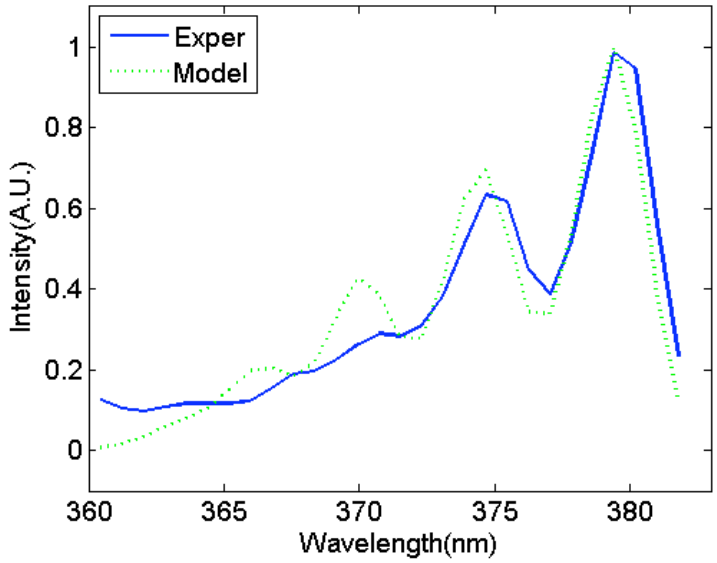

Figure 12. Modeled spectra and the corresponding best-fit for positive column (T_{rot} = 2500 K, T_{vib} = 2000 K)

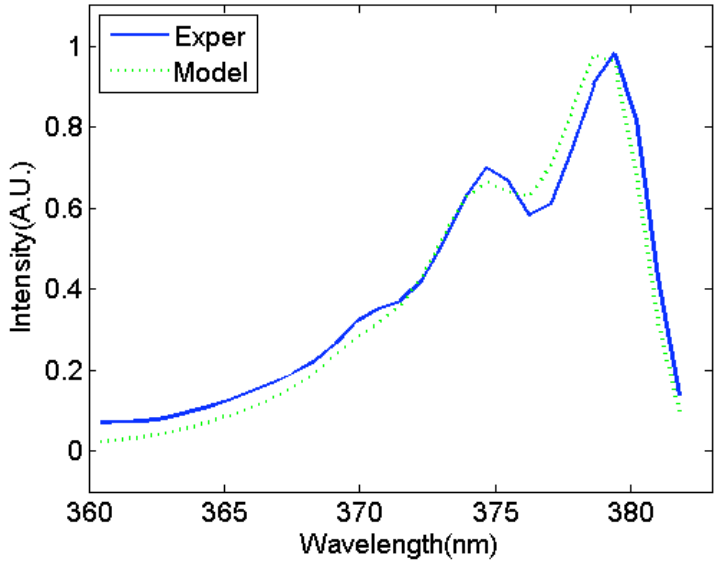

Figure 13. Modeled spectra and the corresponding best-fit for anode glow (T_{rot} = 500 K , T_{vib} = 3000 K)

The experimental spectra were shifted by 0.9 nm towards the short-wavelength end of the wavelength axis to better match with the modeled spectra. From the simulation

results shown in p.24 and p.25 above, the best-fit temperatures for the positive column were T_{rot} = 2500 K, T_{vib} = 2000 K. For the cathode glow column, T_{rot} = 1500 K, T_{vib} = 3000 K, and for the anode glow they were T_{rot} = 500 K, T_{vib} = 3000 K. The accuracy of the rotational temperature estimated was ± 500 K since we used SPECAIR data with T_{rot} at increments of 500 K. The rotational temperature in the positive column was the highest. This is probably due to the fact that most of the plasma voltage drop takes place in this region and the primary heat-loss mechanisms are limited to convection and radiation. On the other hand, the anode glow is in close contact with the room-temperature rock surface, which helps to explain its lower temperature. In the next section, we will discuss the absolute calibration for our spectroscopic system.

IV. ABSOLUTE CALIBRATION OF SPECTROSCOPIC SYSTEM

Another important issue is the calibration of the spectroscopic system. The absolute calibration technique will enable us to measure experimental spectral irradiance $\xi_x(\lambda_i)$ (μW cm^{-2} nm^{-1}) and spectral radiance $L_x(\lambda_i)$ (μW cm^{-2} nm^{-1} sr^{-1}). A QE65000 spectrometer and a re-imager were used to record the spectra of sources. A re-imager used a 75% reflectivity beam splitter mirror that deflects most of the light to two planoconvex lenses, concentrating light in 25 mm column down to end of 1 mm diameter fiber-optic cable. A standard lamp (LS-1-CAL) was used to calibrate the spectrometer for which spectral irradiance as a function of wavelength is provided by the manufacturer over the wavelength range from 300 nm to 1050 nm, at 10 nm intervals. Using the 1-mm fiber optic cable and the QE65000 spectrometer, we obtained a spectrum from the LS-1-CAL after it has warmed up for the prescribed amount of time, i.e., 30 minutes. A dark spectrum was recorded with the same exposure time and subtracted from the measured spectrum to eliminate dark current. This gave a dark-compensated data set $C_{CAL}(\lambda_i)$ for the standard exposure time τ. The setup as shown in Figure 14 was used.

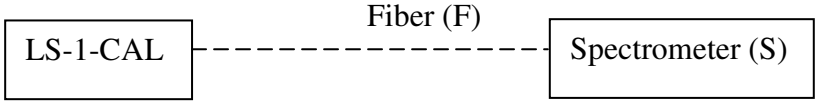

Figure 14. Fiber-optic cable directly connects LS-1-CAL unit with the spectrometer

The re-imager is put on a transit level and aligned with the constant-source using a laser. A flashlight bulb operating at a constant voltage of 3.98 V is used as a constant source light. We approximate the angular response of the re-imager by measuring its relative output in counts averaged over the usable bandwidth as its response to a distant constant-output source varies with angle. So, the wavelength dependence of the angular response is included only in an average sense, not explicitly.

The following setup was used:

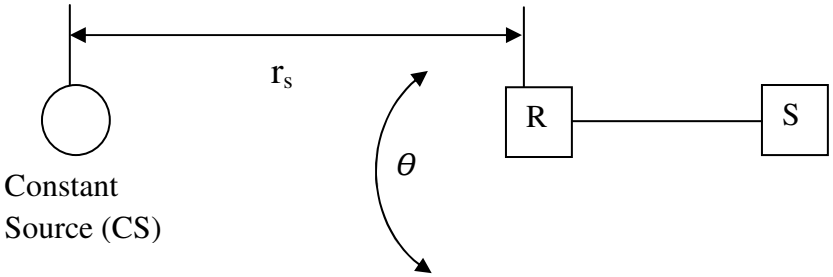

Figure 15. Re-imager over transit level used to take spectrum at different θ_i

If we let the count array for a given angle θ_k (k=1 to M) be $C(\lambda_i, \theta_k)$, we can perform the approximate average over the wavelength range by forming the sum of the pixel counts:

$$\sum\nolimits_R (\theta_k) = \sum_{i=1}^{N} C_R(\lambda_i, \theta_k) \tag{3}$$

This is the weighted average whose weights depend on the spectrum of the constant source. This is the best we can do without a special source. If the wavelength variation with angle is not large, the averaging will not contribute a significant error. The counts as a function of angle for the re-imager are denoted as $C_R(\lambda_i, \theta_k)$. The normalized angular response function of the re-imager is

$$S_R(\theta) = \frac{\sum_R(\theta)}{\sum_R \max} \tag{4}$$

The conversion factor K_i is calculated from the fiber cross-sectional area A (cm^2), the calibration data file $\xi_{CAL}(\lambda_i)$ ($\mu W\ cm^{-2}\ nm^{-1}$) supplied with the LS-1-CAL unit, the count array $C_{CAL}(\lambda_i)$ resulting from the experiment of Figure 14, and the maximum value of the count array C_{MAX}.

$$K_i = A\xi_{CAL}(\lambda_i)\frac{C_{MAX}}{C_{CAL}(\lambda_i)}\ (\mu W\ nm^{-1}) \tag{5}$$

Now all count data can be converted to equivalent power data using (6)

$$P_*(\lambda_i) = K_i\frac{C_*(\lambda_i)}{C_{MAX}}\ (\mu W\ nm^{-1}) \tag{6}$$

The symbol * stands for R, or X (re-imager measurements of experiment on Figure 15 or the actual experimental data). Assuming that the constant source's solid angle as viewed by the re-imager in experiment in Figure 15 is so small that the angular response function S_R is constant over the solid angle, we can determine the constant source's irradiance.

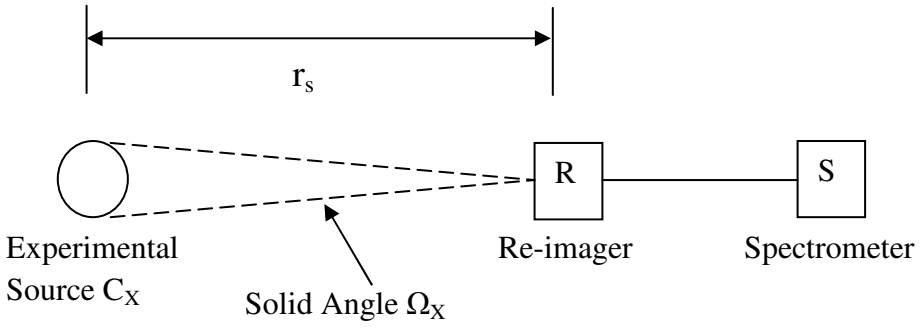

Figure 16. Experimental setup to measure solid angle

For a given spectral irradiance ξ (μW cm^{-2} nm^{-1}) arriving at an angle θ to the re-imager's optical axis, the re-imager will send a power $A_{RE}(\theta)\xi(\lambda_i)\Delta\lambda_i$ (μW) into the fiber. We can now compute the effective area of the re-imager $A_{RE}(\theta)$ as shown in (7) below:

$$A_{RE}(\theta) = A\frac{\xi_{CAL}(\lambda_i)C_R(\lambda_i,\theta)}{C_{CAL}(\lambda_i)\xi_{CS}(\lambda_i)} \tag{7}$$

With the experimental setup shown in Figure 16 which produces an experimental data array $C_X(\lambda_i)$, the equation to find the experimental spectral irradiance $\xi_X(\lambda_i)$ (μW cm^{-2} nm^{-1}) as received at the re-imager input port was then computed using (8) as follows:

$$\xi_X(\lambda_i) = \frac{A}{A_{RE}(\theta_{MAX})}\frac{C_X(\lambda_i,\theta_{MAX})}{C_{CAL}(\lambda_i)}\xi_{CAL}(\lambda_i) \tag{8}$$

The effective solid angle (in steradians) of the re-imager is then given by (9).

$$\Omega_R = 2\pi\int_{\theta=0}^{\pi/2} S_R(\theta)\sin(\theta)d\theta \tag{9}$$

The spectral radiance L of the source is then given by dividing equation (8) by equation (9).

In sum, the goal of this study was to enable us to measure field quantities such as experimental spectral irradiance and experimental spectral radiance using the re-imager when connected through the 1-mm fiber cable. This procedure took into account the directional properties of the re-imager-fiber-spectrometer combination.

V. DISCUSSIONS

Plasma spectroscopy which focuses on atomic and molecular emission spectra of low temperature plasmas or other light sources is a powerful diagnostic tool. With a very simple experimental set-up it provides a non-invasive diagnostic method. Although spectra are recorded easily, interpretation of those spectra can be a complex task.

Although we did not see any genuine Marfa lights during our 20-night observation, we showed that from the analysis of spectral data we can draw unequivocal conclusions about the origin of all light sources that were bright enough to produce spectra with an adequate signal-to-noise ratio. We used the Fraunhofer A-band due to absorption of molecular oxygen to determine the distances of several continuum-spectrum light sources.

In the second part of the thesis, the atmospheric pressure DC normal glow discharge is discussed. The DC normal-glow discharge's practical applications make it a highly sought-after type of plasma, but virtually all applications of this type of plasma require pressures below atmospheric. We have demonstrated that natural porous rock can support a large-area DC normal glow discharge up to 18 mm in diameter. This finding is unprecedented in the literature. We believe that the rock’s pores have a stabilizing and enlarging effect on the plasma through the air. Temperature measurements, visualization and parametric studies of the discharge show it to be a normal glow discharge. Emission spectroscopy and gas temperature measurements using the 2nd positive band of N_2 indicate that the discharge forms non-equilibrium plasma. Although we have studied only

natural basalt extensively, field studies with a portable high-voltage setup show that the same type of phenomenon can occur with a wide variety of other rocks such as granite. The essential requirements seem to be only that the rocks must have water content in them. Finally, absolute calibration of our spectroscopic system could be implemented based on the mathematical derivations we have presented and this would allow us to compute experimental spectral irradiance and experimental spectral radiance. Due to lack of time and a proper calibrated source, results for absolute calibration for the plasmas could not be completed. All of our spectroscopic analysis was therefore based on relative intensities.

In sum, this research may have important implications for the scientific study of various atmospheric phenomena, such as ball lightning and Marfa lights. Besides, there are many important applications of non-thermal plasmas to the manufacturing of materials such as in the manufacturing of microelectronics and integrated circuits. Plasma processing also plays important role in textile processing and biomedical applications.

REFERENCES

Abrahamson, J., Bychkov, A. V., & Bychkov, V. L. (2002). Recently Reported Sightings of Ball Lightning: Observations Collected by Correspondence and Russian and Ukrainian Sightings. *Philosophical Transactions: Mathematical, Physical and Engineering Sciences, 360*(1790), 11-35.

Bunnell, J. (2009). Marfa Lights Research. Retrieved October 27, 2009, from www.nightorbs.net

Fantz, U. (2006). Basics of plasma spectroscopy. *Plasma Sources Science and Technology, 15*(4), S137.

Garamoon, A. A., & El-zeer, D. M. (2009). Atmospheric pressure glow discharge plasma in air at frequency 50 Hz. *Plasma Sources Science and Technology, 18*(4), 045006.

Hall, M. (2006). The Truth Is Out There. Retrieved October 27, 2009 from http://www.texasmonthly.com/preview/2006-06-01/feature2.

Laux, C. O., Spence, T. G., Kruger, C. H., & Zare, R. N. (2003). Optical diagnostics of atmospheric pressure air plasmas. *Plasma Sources Science and Technology, 12*(2), 125-138.

Pierluissi, J. H., & Tsai, C.-M. (1986). Molecular transmittance band model for oxygen in the visible. *Appl. Opt., 25*(15), 2458-2460.

Staack, D., Farouk, B., Gutsol, A., & Fridman, A. (2005). Characterization of a dc atmospheric pressure normal glow discharge. *Plasma Sources Science and Technology, 14*(4), 700-711.

Stephan, K. D., Ghimire, S., Stapleton, W. A., & Bunnell, J. (2009). Spectroscopy applied to observations of terrestrial light sources of uncertain origin. *American Journal of Physics, 77*(8), 697-703.

Stolyarov, A., Klenzig, J., Roddy, P., & Heelis, R. A. (2005). An experimental analysis of the Marfa lights. Retrieved March 3,2010 from www.spsnational.org/wormhole/utd_sps_report.pdf.

Wark, D. Q., & Mercer, D. M. (1965). Absorption in the Atmosphere by the Oxygen 'A' Band. *Appl. Opt., 4*(7), 839-845.

VITA

Sagar Ghimire was born in Morang district of Nepal on January 9, 1979. He is the son of Dev Kumar Sharma and Shanta Ghimire. After completing his schooling from Hermann Gmeiner School Sanothimi, Bhaktapur, Nepal in 1994 he entered St. Xavier's Campus, Kathmandu, Nepal and completed his Intermediate in Science (I.Sc.) in 1996. He entered Tribhuvan University, Institute of Engineering in 1996 and completed his Bachelor's Degree in Electronics Engineering and Master's in Information and Communication Engineering in the years 2001 and 2005 respectively.

He was working as a Telecom Engineer in Nepal Telecom before he entered the Graduate College of Texas State University-San Marcos in January 2008. During the following years he served as a Graduate Instructional Assistant in the Department of Engineering Technology and Ingram School of Engineering for Circuits and Devices, Digital Electronics, Industrial Electronics, Fields and Waves and Microelectronics Manufacturing labs.

Email: sagarghimire@gmail.com

This thesis was typed by Sagar Ghimire.